

Vacancy-impurity complexes and limitations for implantation doping of diamond

J. P. Goss, P. R. Briddon, and M. J. Rayson

School of Natural Sciences, University of Newcastle upon Tyne, Newcastle upon Tyne, NE1 7RU, United Kingdom

S. J. Sque and R. Jones

School of Physics, University of Exeter, Exeter, EX4 4QL, United Kingdom

(Received 23 March 2005; revised manuscript received 23 May 2005; published 18 July 2005)

Many candidates have been proposed as shallow donors in diamond, but the small lattice constant means that many substitutional impurities generate large strains and thus yield low solubilities. Strained impurities favor complex formation with other defects and, in particular, the lattice vacancy. We report the results of first-principles calculations regarding the geometry, electronic structure, and energetics of impurity-vacancy complexes in diamond and show that such complexes explain the generally low doping efficiency for implanted material.

DOI: [10.1103/PhysRevB.72.035214](https://doi.org/10.1103/PhysRevB.72.035214)

PACS number(s): 61.72.Ji, 61.72.Bb, 71.20.Mq, 71.23.An

I. INTRODUCTION

The optimization and manufacture of wide-gap semiconductors for high-power devices and optoelectronics is a rapidly expanding area. Diamond has extremely favorable intrinsic properties, and *p*-type semiconducting material is achievable via substitutional boron acceptors (B_s). The acceptor level at $E_v+0.37$ eV (Ref. 1) is close to effective mass, and in heavily doped material conduction is metallic.²

However, the current *n*-type dopant of choice, substitutional P (P_s), has a relatively deep donor level [$E_c-0.6$ eV (Ref. 3)], and alternatives, such as sulfur⁴⁻⁶ and boron-deuterium complexes,⁷ remain to be understood. Impurity complexes, such as S-vacancy-H, N-H-N, S-B, and Si_4 -N, are theoretically competitive with phosphorus,⁸⁻¹⁴ but the feasibility of these dopant complexes is unproved.

Theory also suggests that As_s and Sb_s improve on P_s .^{15,16} Indeed, pnictogen and chalcogen dopants yield progressively shallower ($0/+$) levels as the atomic number Z increases. Doping by substitutional donors has an advantage over impurity complexes [such as N_s -H- N_s (Ref. 9), sulfur- X complexes (Refs. 8, 10–13, and 17), and Si_4 N (Ref. 4)] in that they do not rely on complex formation paths, either via growth or post-growth processing. Then doping with As or Sb may be achievable via ion implantation.

Implantation doping of diamond has a rather mixed record. For instance, B-implanted *p*-type material has been obtained¹⁸ and relatively shallow *n*-type conduction [typically 0.2–0.5 eV (Refs. 19–21)] is seen subsequent to donor-impurity implantation. However, in the latter case the “donor level” is weakly dependent on the implanted ion, with *n*-type conduction being obtained using inert-gas and C^+ implants.²² The *n*-type character may be due to hopping conduction via the implantation damage rather than from impurity doping,²³ but it is not clear that this mechanism can be technologically exploited due to the low carrier mobilities and high resistivities.

Additionally, there is evidence that the fraction of donors on substitutional sites subsequent to implantation is typically of the order of 50% or less.^{24,25} Among those on site, many

have unannealed lattice damage close by,²⁵ possibly compensating the dopant. Therefore the formation of complexes with lattice damage is of great importance.

Impurity-vacancy complexes ($X-V$) are often optically and electrically active. N- V is probably the best characterized of these complexes, and its structure is shown schematically in Fig. 1(b). Optical transitions at 1.945 eV and 2.156 eV have been assigned to N- V in the negative- and neutral-charge states, respectively,²⁶⁻²⁹ with the measured ($-/0$) level at $E_c-2.583$ eV.³⁰ The difference between the two charge states is thought to be primarily the occupancy of the “dangling bond” (DB) orbitals on three (equivalent) carbon atoms.²⁶ Indeed, (N- V)⁻ is seen in paramagnetic resonance (labeled W15) with >70% of the unpaired spin located on three carbon atoms.³¹ Due to the deep ($-/0$) level, N- V compensates donors.

A second commonly observed $X-V$ complex contains Si.^{26,32} Si- V gives rise to a characteristic 12-line optical signature around 1.682 eV, with the fine structure due to a transition between two electronic-doublets for the three naturally occurring Si isotopes. Previous calculations²⁶ suggest the optical transition is associated with ² E ground and excited states of (Si- V)⁻, consistent with the ($-/0$) level in the lower half of the band gap.¹⁶ However, experimental data appear to contradict this view,³³ although they remain to be confirmed.

Unlike N- V , Si- V adopts the split-vacancy structure [Fig. 1(c)]. However, the gap levels of Si- V are also strongly lo-

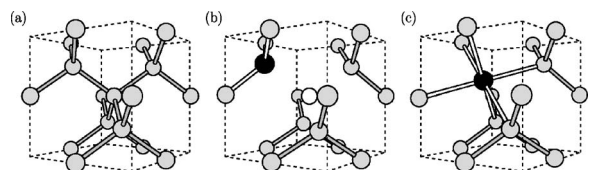


FIG. 1. Schematics of vacancy-impurity complexes in diamond. Black and gray atoms represent the impurity and host atoms, respectively, with the white circle in (b) indicating the vacancy. (b) shows the impurity on a substitutional site neighboring the vacancy, and (c) shows the split-vacancy configuration where an interstitial impurity lies at the center of a divacancy. (a) shows the corresponding section of bulk material for comparison.

calized on the neighboring C atoms, in this case the six carbon atoms neighboring the silicon impurity, and it appears that the electronic structure can then be understood rather simply from the gap states of an ideal (D_{3d} symmetry) divacancy (V_2). (In fact, V_2 in diamond undergoes a complex distortion to C_{2h} symmetry in the neutral, $S=1$ state,^{34,35} but at elevated temperatures the distortion is lost and an effective D_{3d} symmetry is seen.³⁴)

P-V and In-V also theoretically adopt the split-vacancy structure,^{36,37} and S-V, I-V, and Xe-V complexes have been examined theoretically previously. I-V is of particular interest as Anderson *et al.*, using empirical molecular orbital methods, suggested it has a shallow donor behavior.⁸ They found that I-V distorts to C_{2h} symmetry, yielding I-C inter-nuclear distances of 2×2.001 and 4×2.085 Å. However, it should be noted that in the same study the ($0/+$) levels for N_s and P_s were in poor agreement with experiment, and the shallow donor level of I-V remains to be confirmed. Although a number of publications report S-V,^{10,11} there are few data concerning its structure or properties, with greater emphasis being paid to more complex donor systems such as S-V-H₃. Xe (Ref. 8) was predicted to adopt a C_{3v} structure.

Since at least some of the Si and N grown into diamond are incorporated with a vacancy and considering the likelihood of forming such defects in implantation-doped material following an anneal stage, X-V complexes are important for doping. Two critical factors are the binding energy of the vacancy to the dopant and the subsequent electronic properties of the vacancy-impurity complex. Therefore, in this paper we present the results of first-principles calculations for the structure, energetics, and electronic structure of X-V complexes with X being group-III (B, Al, Ga, and In), group-IV (Si, Ge, and Sn), pnictogen (N, P, As, and Sb), chalcogen (O, S, Se, and Te), and halogen (F, Cl, Br, and I) impurities, allowing us to draw some general chemical trends.

II. METHOD

Calculations were carried out using the local-spin-density-functional technique implemented in AIMPRO (Ref. 38) (*ab initio* modeling program). To model the various defects, 64- and 216-atom cubic unit cells of side length $2a_0$ and $3a_0$ have been used. Calculations have been performed with the lattice constant fixed to the theoretical value for bulk diamond, and in addition calculations were performed with the lattice constant allowed to vary such that the energy is minimized. For all systems we employ the Monkhorst-Pack³⁹ scheme for sampling the Brillouin zone, with a mesh of $2 \times 2 \times 2$ special k points folded by taking symmetry into account. For several sample structures we calculated the total energies using a $4 \times 4 \times 4$ mesh, which indicated that the absolute total energies are converged to 10 meV or better for both cell sizes. Structures are optimized via a conjugate-gradient scheme until the total energy changes by less than 10^{-5} Ha. This cannot guarantee that the structures are global minima, but by relaxing from different starting points and obtaining similar end-point structures, we gain some confidence that structures and energies presented in this paper are

reasonable representations of the ground states.

Norm-conserving pseudopotentials⁴⁰ eliminate core electrons. The pseudo-wave-function basis consists of independent sets of s , p , and d Gaussian orbitals centered at each atomic site. The charge density is Fourier transformed using a basis of plane waves with an energy cutoff of 300 Ry. Doubling the cutoff changes the total energy by 1 meV or less. The lattice constant and bulk modulus of bulk diamond using these parameters are within $\sim 1\%$ and 5% , respectively, of the experimental values, while the direct and indirect band gaps are in close agreement with previously published plane-wave local-density-approximation (LDA) values⁴¹ (5.68 and 4.18 eV).

We use the definition for the formation energy of neutral system X as

$$E^f(X) = E(X) - \left(\sum_i^{\text{atoms}} \mu_i \right), \quad (1)$$

where μ_i are the chemical potentials of the atomic species and $E(X)$ is the calculated total energy. The binding energy (E^b) of complex AB is the energy liberated in the reaction $A+B \rightarrow AB$.

The calculated electrical levels compare electron affinities or ionization energies of different systems.⁴² The details are given elsewhere,¹⁶ as are the computational details for the calculation of zero-field splittings.^{43,44}

III. RESULTS

For each chemical species considered, we have calculated the structure and energy of X_s and X-V. We begin by summarizing the results for X_s .

A. Substitutional site

1. Group-III acceptors

B_s undergoes a distortion to C_{3v} symmetry, with one B—C bond being shorter than the others.⁴⁵ The asymmetry is due to the preferential depopulation of one bonding orbital, in line a static Jahn-Teller effect detected with Zeeman spectroscopy.⁴⁶ B_s^- lies on site (T_d symmetry), but with B—C bonds around 2% longer than bulk C—C bonds. We find that the other group-III impurities examined lie on site in both neutral- and negative-charge states, and exert a compressive strain on the surrounding material. All four neutral defects introduce partially filled bands split off from the valence-band top, rising in energy with increasing atomic number.

2. Group-IV impurities

Group-IV impurities lie on site and lead to a large compression of the surrounding lattice. Because Si, Ge, and Sn are isoelectronic with the host, the only effect they have on the electronic structure is to push occupied states above the valence-band top. Our results agree qualitatively with previous calculations for Si_s .^{14,47}

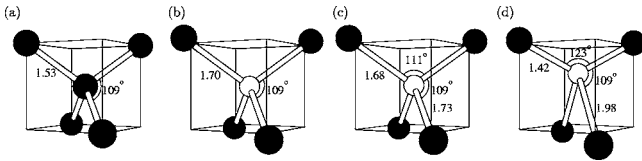


FIG. 2. Three low-energy structures for O_s in diamond. Black and white circles represent C and O atoms, respectively. (b) T_d , (c) C_{2v} , $S=0$, and (d) C_{2v} , $S=1$. Bond lengths in Å. (a) shows the corresponding section of bulk material.

3. Pnictogens

Our calculated electronic and geometric properties for pnictogens have been presented previously.¹⁵ Briefly, in the neutral-charge state N is significantly displaced off site along $\langle 111 \rangle$, producing an elongated X-C bond,⁴⁸ with a much smaller symmetry-lowering distortion seen for P, As and Sb were found to remain on site.

4. Chalcogens

Previously we reported¹⁵ that chalcogens undergo a small distortion along $\langle 111 \rangle$, so that one of the four neighboring C atoms is farther from the impurity than the other three.

In addition, we have also investigated oxygen. Diamagnetic O_s^0 with T_d , C_{3v} (elongated bond along $\langle 111 \rangle$), and C_{2v} (displaced along $[001]$) symmetries all have the same total energy to within a fraction of a meV. This is likely to be a consequence of a rather flat energy surface for the O atom in the vicinity of the tetrahedral site. Interestingly, a $S=1$, C_{2v} configuration is also degenerate in energy, but with a larger displacement along $\langle 100 \rangle$ (Fig. 2). We find the $S=1$ configuration very slightly lower in energy, but the energy difference at around 2 meV is too small to conclude that this is the true ground state. We note that previous density functional calculations found O_s to lie on site, but it is unclear if the $S=1$ was considered.⁴⁹

Unlike the larger chalcogen defects, the Kohn-Sham band structure indicates midgap defect levels, rendering O_s both a donor and acceptor. The C_{2v} structure is strongly preferred in the negative-charge state.

The on-site defect has two levels in the gap. The lower is filled and has a_1 symmetry. The upper has t_2 symmetry and in the neutral-charge state is unoccupied. The addition of electrons in the negative-charge state or the neutral $S=1$ configuration renders the defect a candidate for a Jahn-Teller distortion. In the C_{2v} -distorted case, the t_2 level is split into $b_1 a_1^* b_2$, with only the b_1 and a_1^* levels, split by ~ 2 eV at the zone center, lying in the band gap (the b_2 level being inferred from group theory must lie in the conduction band on electron counting grounds). The a_1 and b_1 levels are chiefly even and odd combinations of carbon dangling bonds, respectively, leaving oxygen to participate in a divalent interaction with the two close-by neighbors. This is the structure for the $S=1$ excited state of the A center in silicon, VO^* .⁵⁰

Other chalcogens do not undergo this distortion because the compression of the surrounding lattice inhibits large displacements of the impurity atoms from the lattice site. Additionally, S, Se, and Te only possess the occupied a_1 level in

the band gap. The distortion to C_{3v} symmetry localizes this level more on a single bond, analogous to N_s . The C_{3v} form of X^+ is most stable, with all chalcogens on site in the +2-charge state.

5. Halogens

F_s^0 (isoelectronic with O_s^-) also undergoes a distortion to orthorhombic symmetry, lowering the total energy by around 0.4 eV relative to the on-site case. Cl and Br relax to trigonal structures, and iodine adopts a C_{2v} structure. For the larger impurities the energy difference between different off-site symmetries is small; for example, the C_{2v} and C_{3v} structures differ by 0.05, 0.14, and 0.11 eV for Cl, Br, and I, respectively. It is therefore likely that these defects will possess a motionally averaged T_d symmetry at elevated temperatures.

The neutral halogens are paramagnetic, $S=1/2$ systems, and we note also that F_s^- adopts a $S=1$ ground state. If present in sufficient quantities these defects represent candidates for observation in electron-paramagnetic resonance (EPR) experiments, with the advantage that all halogens have nuclear spins for chemical identification via the hyperfine interactions.

Geometric and electronic properties of X_s are summarized in Table I. The calculated $(0/+)$ and $(-/0)$ levels are obtained by comparing the electron affinity and ionization energies of the defects with the values obtained for bulk diamond supercells of the same size. Of these defects, electrical levels have been measured unambiguously only in the cases of B, N, and P, with levels at $E_v+0.37$,¹ $E_c-1.7$,⁵² and $E_c-0.6$,³ respectively. Calculated values for these are in close agreement, giving confidence in the other calculated electrical levels.

The lack of space in diamond means that there is considerable displacement of nearest neighbors in most cases. This will affect the lattice constant and energetics of these systems, and is explored in Sec. III B 5.

B. X-V complexes

1. Atomic geometries

For all impurities, we have optimized the X-V complexes starting from structures (b) and (c), Fig. 1. We have also considered perturbed versions of (b) where two equivalent carbon neighbors to X are moved closer to the impurity, lowering the symmetry to C_{2h} in line with the predicted structure⁸ of $(I-V)^0$. This distortion is unstable for all species. Furthermore, we have commenced optimization from a distorted structure with no symmetry and, with the exception of F-V, we find relaxed structures indistinguishable from the trigonal forms.

We find a clear division between impurities that adopt structures (a) and (b) in Fig. 1. First-row impurities, which have a covalent radius similar to that of carbon (Table I), adopt (a), and all others adopt (b). For B, N, O, and F we have additionally calculated the energy difference between structures (a) and (b) to be 1.14, 4.76, 2.71, and 0.7 eV, respectively.

TABLE I. Nearest-neighbor (NN) bond lengths and average distances to the next-nearest neighbors (NNN) for neutral X_s defects in diamond as calculated using a 64-atom cubic supercell expressed as a multiple of bulk C-C distances. Also listed are the point-group symmetries we find for the ground state in each case, as well as the covalent radius (Ref. 51) R (Å).

X	Structure			Electrical levels		R
	Sym.	NN	NNN	(0/+)	(-/0)	
B	C_{3v}	1.03, 1.02	1.00	—	$E_v+0.5^a$	0.88
Al	T_d	1.15	1.01	—	$E_v+1.4^b$	1.26
Ga	T_d	1.16	1.01	—	$E_v+1.4^b$	1.26
In	T_d	1.21	1.02	—	$E_v+1.8^b$	1.44
C						0.77
Si	T_d	1.12	1.02	—	—	1.17
Ge	T_d	1.14	1.02	—	—	1.22
Sn	T_d	1.20	1.03	—	—	1.40
N	C_{3v}	0.96, 1.30	1.01	$E_c-1.5^a$	$E_c-1.1^a$	0.70
P	C_{3v}	1.09, 1.12	1.02	$E_c-0.3^a$	—	1.10
As	T_d	1.15	1.02	$E_c-0.0^a$	—	1.18
Sb	T_d	1.22	1.03	$E_c+0.2^a$	—	1.36
O	T_d	1.11	1.00	$E_c-2.8^a$	$E_c-1.9^a$	0.66
S	C_{3v}	1.10, 1.24	1.01	$E_c-1.2^a$	—	1.04
Se	C_{3v}	1.17, 1.30	1.02	$E_c-1.0^a$	—	1.14
Te	C_{3v}	1.24, 1.33	1.03	$E_c-0.7^a$	—	1.32
F	C_{2v}	1.06, 1.28	1.01	$E_c-3.0^b$	$E_c-1.9^b$	0.64
Cl	C_{3v}	1.16, 1.35	1.01	$E_c-2.1^b$	$E_c-1.3^b$	0.99
Br	C_{3v}	1.22, 1.35	1.02	$E_c-1.7^b$	$E_c-0.9^b$	1.11
I	C_{2v}	1.28, 1.29	1.04	$E_c-1.2^b$	$E_c-0.4^b$	1.28

^aReference 16.

^bThis work.

The bond lengths are summarized in Table II. The displacement of the surrounding material in the X - V complexes is much smaller than that seen for the substitutional impurities (Table I), with the maximum deviation from the “ideal” distances being just 7%. This lowering of the local strain by complex formation has obvious implications for the formation energy of the complexes relative to the substitutional defects, as discussed below (Sec. III B 5).

The only structure we find with lower than trigonal symmetry is F- V : F is displaced along [001] from the trigonal axis, rendering the final symmetry C_s , so that F has neighbors at 93% and 133% of the bulk C—C distance. The total

energy is around 0.4 eV lower than the C_{3v} structure and can be viewed as V_2F , with F saturating a single DB.

2. Electronic structure

The electronic structure of X - V centers can be understood to a significant degree by modifying those of V and V_2 , and we discuss each in turn.

V can be described simply by a set of linear combinations of four DB orbitals, yielding states with a_1 and t_2 symmetry.⁵³ Each C neighbor donates one electron, yielding four electrons in the neutral vacancy in a $a_1^2 t_2^2$ configuration from which four multiplets are formed.

TABLE II. Nearest-neighbor bond lengths for neutral X - V defects in diamond as calculated using a 64-atom cubic supercell listed as a multiple of the bulk-diamond distances [$\sqrt{3}a_0/4$ and $\sqrt{19}a_0/8$ for structures (a) and (b), respectively].

X	B	Al	Ga	In	Si	Ge	Sn
X-C	1.01	1.04	1.05	1.07	1.02	1.04	1.07
X	N	P	As	Sb	O	S	Se
X-C	0.95	1.01	1.03	1.07	1.00	1.00	1.03
X	F	Cl	Br	I			
X-C	0.93	1.04	1.05	1.08			

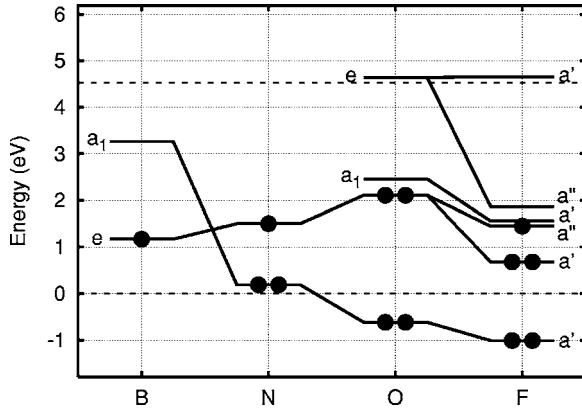


FIG. 3. Schematic of the X-V defect-related Kohn-Sham states in the vicinity of the band gap for first-row elements. Horizontal dashed lines indicate the location of the valence (0 eV) and conduction bands at the Brillouin-zone center. Dots indicate occupancy.

A neighboring impurity X lowers the symmetry from T_d to C_{3v} , splitting the t_2 levels into a_1 and e . The ordering of these levels depends on X : the a_1 orbital is associated with the impurity atom. Accordingly, for B, which is less electronegative than C, the B-related a_1 orbital is empty and the electronic configuration is $a_1^2 e^1 a_1^0$. In contrast, for N the a_1 level is a filled lone pair and the configuration is $a_1^2 a_1^2 e^1$, consistent with the 2E ground state seen optically for this defect.²⁸

Oxygen also has a low-energy filled lone pair, yielding $a_1^2 a_1^2 e^2$, isoelectronic with $(N-V)^-$. In addition to the vacancy-related states, however, there are empty bands higher in the gap, and O-V has an electronic configuration $a_1^2 a_1^2 e^2 a_1^0 e^0$. The additional states reside predominantly on the O—C bonds.

The one-electron configuration leads to three many-body wave functions (1A_1 , 3A_2 , and 1E) but it is not possible to accurately predict the multiplet splittings using the methods employed in this study. We have taken the approach of treating each spin configuration with a single-determinantal wave function. This means that the $S=0$ energy includes contributions from 1A_1 and 1E multiplets, and we cannot predict the ground-state effective spin with certainty. However, for $(N-V)^-$ this approach yields a splitting of around 0.5 eV in comparison to 0.44 eV calculated previously using the von Barth procedure where the spin splitting is estimated more accurately.²⁶ This gives us some confidence in the results obtained in this study. The spin splittings calculated for $(B-V)^-$ and $(O-V)$ also favor $S=1$ by 0.5 eV, and thus we predict these centers to be EPR active.

The F-V complex differs from B, N, and O due to the distortion to C_s symmetry. However, there is a simple correlation with the trigonal electronic configuration of $(O-V)^-$, but with the degenerate representations splitting into nondegenerate pairs: $a_1^2 a_1^2 e^3 a_1^0 e^0 \rightarrow (a')^2 (a'')^2 (a''')^2 (a''')^1 (a''')^0 (a''')^0 (a')^0$.

The electronic structure of the first-row element neutral X-V centers is shown in Fig. 3. Here we have taken the average of the spin-up and spin-down orbital energies at a representative point in the Brillouin zone. This shows the trend for the gap states to drop in energy as Z increases.

We now turn to the second class of X-V centers. As with the monovacancy, the electronic structure of the D_{3d} diva-

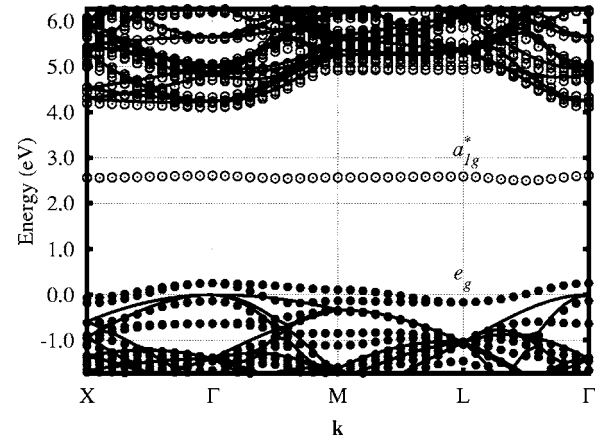


FIG. 4. The band-structure of $(S-V)^0$ in diamond in the vicinity of the band gap along high-symmetry directions in the cubic Brillouin zone of the 215-atom cubic supercell. The solid and open circles indicate occupied and empty bands, respectively. The energy scale is defined such that the valence band top is at zero. The solid lines show the band structure for the 216-atom bulk cell for comparison. The bands with e_g and a_{1g}^* symmetry at Γ are labeled.

cancy can be generated from linear combinations of the six DB orbitals.⁵⁴ Taking one electron from each carbon atom results the neutral configuration $a_{1g}^2 a_{2u}^2 e_u^2 e_g^0$. The addition of group-III to group-VI impurities adds three to six electrons to these orbitals, yielding $a_{1g}^2 a_{2u}^2 e_u^4 e_g^n$ ($n=1-4$). In addition to these orbitals, an a_{1g}^* band is introduced in the upper part of the band gap in some cases. Indeed, this state is necessary to accommodate all the valence electrons of neutral halogen-V complexes.

Mulliken population analysis reveals that the a_{1g}^* level is more localized on the impurity atom than the lower-lying levels. We can take as an example the S-V complex, for which the band structure is shown in Fig. 4. The total electron populations on the six neighboring carbon atoms is comparable for each of the e_g wave functions and the a_{1g}^* state. However, the population on sulfur in a_{1g}^* is s like and around twice that of e_g . We conclude that this state arises chiefly from an antibonding combination of the sp^3 DB's on the carbon with the $3s$ on sulfur. Indeed, halogen-V complexes also have empty gap states (e_u^* and a_{2u}^*) which have the appearance of combinations of $3p$ orbitals on the impurities coupled to the DB's on the six neighboring C atoms.

The locations of the Kohn-Sham band-gap levels for the split-vacancy structures are shown schematically in Fig. 5. As before, we have taken the average of the spin-up and spin-down energies at a representative point in the Brillouin zone.

We note that for $n=2$ we have a similar multiplet issue to that described for O-V. This applies to group-IV elements, negatively charged group-III species, and positively charged pnictogens. In all cases the $S=1$ configuration is found to be favored, but only by around 0.2–0.3 eV.

3. Optical activity

Since the local-density-functional approach does not readily provide a quantitative analysis of the optical transi-

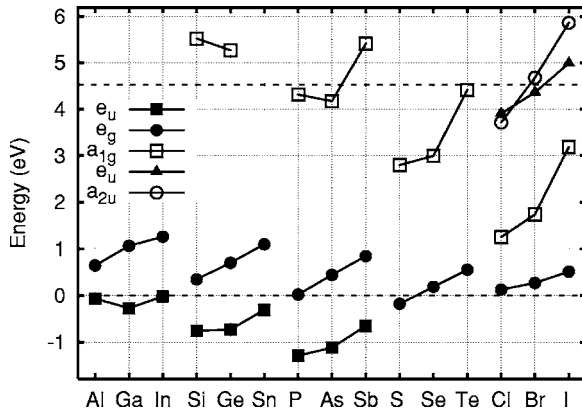


FIG. 5. Schematic of the defect-related Kohn-Sham states in the vicinity of the band gap for elements in split-vacancy structures. Horizontal dashed lines indicate the location of the valence (0 eV) and conduction bands at the Brillouin-zone center. In the neutral-charge state shown, the e_g level (solid circles) accommodates one, two, and three electrons for the group-III, group-IV, and pnictogen elements and is filled for the chalcogens and halogens. The a_{1g}^* level is partially filled for the halogens.

tions, we use the Kohn-Sham spectra in an attempt to obtain a qualitative picture.

The transitions associated with structure Fig. 1(a) can be understood from Fig. 3. In particular, the $e \leftrightarrow a_1$ dipole-allowed transitions at N-V are reasonably represented by the Kohn-Sham splitting. Indeed, the presence of band-gap states suggest that all first-row elements will be optically active in X-V complexes.

Neutral split-vacancy complexes containing group-III, group-IV, and pnictogen impurities are also expected to be optically active, with dipole-allowed transitions occurring between the e_u and e_g levels. Indeed, this is a model for the 1.682 eV Si-related luminescence, albeit in the negative-charge state.²⁶ The energy between Kohn-Sham levels is relatively insensitive to impurity species, suggesting that centers such as Al-V, Ge-V, and P-V might have zero-phonon transitions with an energy in the same spectral region as observed for Si-related luminescence.

Note that the presence of an empty a_{1g}^* level in the gap *does not* render the neutral chalcogen-V optically active since the dipole selection rules prevent direct excitation processes between e_g and a_{1g}^* levels and we find the e_u level to be deep inside the valence band. This lack of an obvious radiative channel may explain the lack of characteristic optical transitions in S-doped material.

Halogen-vacancy complexes (Cl, Br, and I) might undergo excitations involving the a_{1g}^* with empty e_u and a_{2u} bands lying close to the conduction band (Fig. 5). The Kohn-Sham eigenvalues suggest that such processes would be relatively high in energy compared to the known optical transitions associated with N-V and Si-V.

4. Donor and acceptor levels

X-V electrical levels have been calculated using an empirical “marker” method.^{16,42} We use B_s and P_s as the reference acceptor and donor, respectively. The results are listed

in Table III, with the trends shown graphically in Fig. 6. The (0/+) and (-/0) levels, especially among those that adopt the split-vacancy structure, show clear chemical trends: the profile of the donor and acceptor levels moving from group III to group VI is the same for the second, third, and fourth rows of the periodic table. However, the key result is that *all* X-V complexes, with the possible exception of Te-V, will compensate shallow donors.

5. Formation and binding energies

Table III lists formation energy differences

$$\Delta E^f = E^f(X_s) - E^f(X-V),$$

with μ_C taken from bulk diamond. The sign of ΔE^f indicates whether X would preferentially adopt X_s ($\Delta E^f < 0$ eV) or X-V ($\Delta E^f > 0$ eV) in thermodynamic equilibrium. The first-row elements, as well as isoelectronic Si and Ge, are more stable as X_s , with the reverse being true for all other impurities covered in this study.

The binding energy of V to X_s differs from ΔE^f by $E^f(V)$ as

$$E^b(X-V) = E^f(V) + \{E^f(X_s) - E^f(X-V)\}.$$

Since the multiplet energies of V^0 are difficult to calculate accurately, we have taken $E^f(V) = 6$ eV from recent quantum Monte Carlo calculations.⁵⁵

The general trend, as one might expect, is that ΔE^f (and hence E^b) increases with impurity size (R in Table I). The majority of “large” impurities yield $E^f(X-V) < E^f(X_s)$, and then, provided that the formation energies at the surface are similar to the bulk values, one would expect most impurities not to incorporate substitutionally.

However, care has to be taken in such an interpretation. For instance, P is substitutional in as-grown chemical-vapor-deposition (CVD) material, indicating surface-related mechanisms. Indeed, there is theoretical evidence that the formation energy for P at the {111} surface may be substantially lower than in bulk.⁵⁶ We calculate that the difference in *bulk* formation energies for P-V and P_s using the 64-atom supercell is just 1.2–1.5 eV. This is relatively small given the ~ 6 eV variation in $E^f(P_s)$ as a function of depth from a {111} surface.⁵⁶

The equilibrium (theoretical) lattice constant was used in the preceding results, but impurities lead to changes in this parameter. Therefore we have calculated the E^f where a zero-hydrostatic-pressure boundary condition is applied. Mostly the energy change (E^{volume} , Table III) is relatively modest. Since $E^{\text{volume}}(X-V) < E^{\text{volume}}(X_s)$, this leads to a reduced binding energy ($E^{b'}$, Table III).

For the largest impurities the volume effects are quite large in the 64-atom systems, so we also considered larger supercells. The values calculated for E^b are 8.8, 8.2, 12.7, and 15.6 eV for In-V, Sn-V, Sb-V, and Te-V, respectively, in the 216-atom supercell, with $E^{b'}$ being 8.7, 8.1, 12.5, and 15.3 eV. The proportional differences between the 64- and 216-atom cells are relatively small ($\leq 8\%$), and qualitatively the results are independent of cell size. Additional support for this view is gained from the volume displacements in the

TABLE III. Calculated data for $X-V$ complexes in diamond. $(0/+)$ and $(-/0)$ refer to donor and acceptor levels relative to the valence-band top, and U is the energy between these levels. $\Delta E^f = E^f(X_s) - E^f(X-V)$, and E^b is relative to neutral X_s and a neutral vacancy. E^{volume} is the decrease in total energy when the volume of the supercell is relaxed for $X_s(X-V)$, and the binding energy adjusted for the volume relaxation (and change in total energy) of both components is $E^{b'}$. The volume displaced by the presence of $X_s(X-V)$ is listed as ΔV in units of $a_0/8$ of bulk diamond (the volume per host atom), so that volume displaced by a carbon atom is zero by definition; i.e., the equilibrium volume of the 64-atom supercell is $8a_0^3 + \Delta V$. S is the calculated ground-state effective spin. All energies in eV.

X	Sym.	S	$(0/+)$	$(-/0)$	U	ΔE^f	$E^b(X-V)$	E^{volume}	$E^{b'}(X-V)$	ΔV
B	C_{3v}	1/2	0.9	1.6	0.7	-4.2	1.8	0.0 (0.0)	1.8	0.3(0.3)
Al	D_{3d}	1/2	0.7	1.3	0.7	0.4	6.4	0.3 (0.0)	6.1	0.2(-0.3)
Ga	D_{3d}	1/2	1.0	1.7	0.7	0.6	6.6	0.4 (0.1)	6.3	0.6(-0.1)
In	D_{3d}	1/2	1.2	1.9	0.7	2.8	8.8	0.8 (0.2)	8.2	1.0(0.6)
Si	D_{3d}	1	0.3	1.4	1.1	-1.6	4.4	0.3 (0.0)	4.1	1.7(0.7)
Ge	D_{3d}	1	0.6	1.8	1.2	-1.1	4.9	0.4 (0.1)	4.6	1.6(0.5)
Sn	D_{3d}	1	0.9	2.1	1.2	2.3	8.3	1.0 (0.4)	7.7	1.5(0.3)
N	C_{3v}	1/2	1.2	2.0	0.9	-2.5	3.5	0.2 (0.0)	3.3	1.6(0.1)
P	D_{3d}	1/2	0.3	1.0	0.7	1.5	7.5	0.3 (0.0)	7.2	2.0(0.5)
As	D_{3d}	1/2	0.7	1.4	0.7	3.0	9.0	0.5 (0.1)	8.6	1.8(0.8)
Sb	D_{3d}	1/2	1.0	1.7	0.7	6.4	12.4	1.2 (0.3)	11.5	1.8(0.8)
O	C_{3v}	1	1.6	3.1	1.5	-1.3	4.7	0.0 (0.0)	4.7	2.0(0.9)
S	D_{3d}	0	0.0	3.3	3.3	4.3	10.3	0.3 (0.0)	10.0	2.4(0.8)
Se	D_{3d}	0	0.3	3.5	3.2	6.4	12.4	0.6 (0.1)	11.9	2.7(1.2)
Te	D_{3d}	0	0.7	4.8	4.1	10.0	16.0	1.3 (0.4)	15.1	2.6(1.5)
F	C_s	1/2	1.2	2.2	1.0	-1.7	4.3	0.1 (0.0)	4.2	2.9(1.8)
Cl	D_{3d}	1/2	1.1	2.0	0.9	4.0	10.0	0.5 (0.1)	9.6	3.1(1.7)
Br	D_{3d}	1/2	1.6	2.4	0.8	6.3	12.3	0.9 (0.2)	11.6	3.4(1.9)
I	D_{3d}	1/2	3.0	3.7	0.7	9.7	15.7	1.4 (0.6)	14.9	3.6(2.2)

two cell sizes which agree very well: in the 216-atom supercell, ΔV is 2.5, 2.8, 3.0, and 3.3 for In_s , Sn_s , Sb_s , and Te_s , respectively, and 1.5, 1.7, 1.8, and 1.9 for their respective vacancy complexes (cf. Table III).

As with the electrical levels, chemical trends are also present in the binding energies, as illustrated in Fig. 7. For each row of the periodic table there is generally a minimum

for the group-IV elements, with the binding energy then increasing monotonically for groups V, VI, and VII. This diagram includes a point for carbon, which has a binding energy of zero by definition. For each column of the periodic table, E^b increases with increasing Z , as one would anticipate based on notions of atom size.

The binding energies considered thus far relate to *neutral* species—i.e., the energy liberated in the reaction

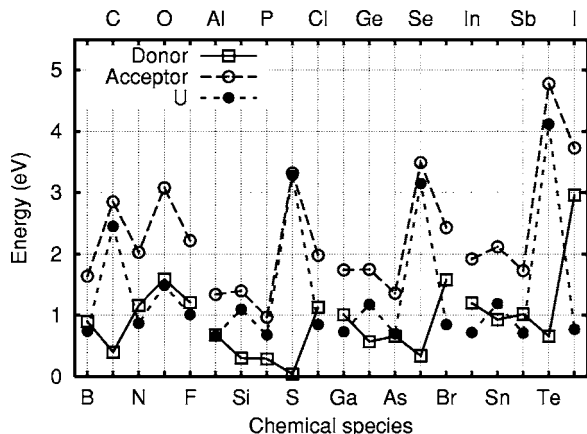


FIG. 6. A plot of the electrical levels of $(X-V)$ in 64-atom supercells, showing the chemical trends. The values for C represent the isolated vacancy, for which the levels derived in Ref. 16 are used. U is the energy difference between the donor and acceptor states for each defect.

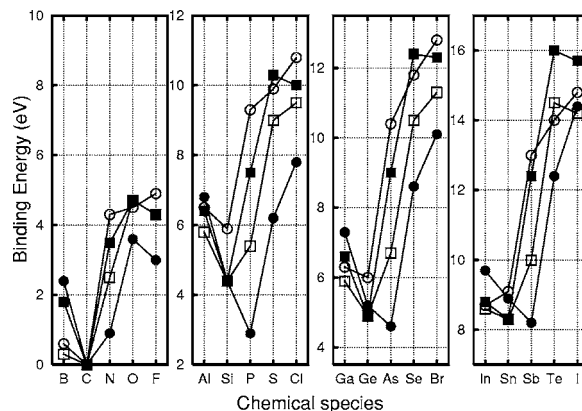
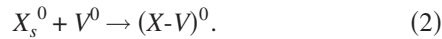


FIG. 7. A plot of the binding energies of $(X-V)$ complexes illustrating the chemical trends. The solid and open squares represent the binding energy for $(X-V)^0$ with respect to neutral and charged components, respectively. The solid and open circles represent the binding energy for $(X-V)^+$ and $(X-V)^-$ (Table IV).

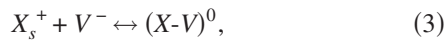
TABLE IV. Calculated binding energies for charged $X-V$ complexes in diamond (eV). All reactions listed are exothermic.

Reactants	Product	E^b	Reactants	Product	E^b		
B_s^-	V^0	(B-V) ⁻	0.6	B_s^0	V^+	(B-V) ⁺	2.4
N_s^0	V^-	(N-V) ⁻	4.3	N_s^+	V^0	(N-V) ⁺	0.9
O_s^0	V^-	(O-V) ⁻	4.5	O_s^+	V^0	(O-V) ⁺	3.6
F_s^0	V^-	(F-V) ⁻	4.9	F_s^+	V^0	(F-V) ⁺	3.0
Al_s^-	V^0	(Al-V) ⁻	6.5	Al_s^0	V^+	(Al-V) ⁺	6.8
Si_s^0	V^-	(Si-V) ⁻	5.9	Si_s^0	V^+	(Si-V) ⁺	4.4
P_s^0	V^-	(P-V) ⁻	9.3	P_s^+	V^0	(P-V) ⁺	2.9
S_s^0	V^-	(S-V) ⁻	9.9	S_s^+	V^0	(S-V) ⁺	6.2
Cl_s^0	V^-	(Cl-V) ⁻	10.8	Cl_s^+	V^0	(Cl-V) ⁺	7.8
Ga_s^-	V^0	(Ga-V) ⁻	6.3	Ga_s^0	V^+	(Ga-V) ⁺	7.3
Ge_s^0	V^-	(Ge-V) ⁻	6.0	Ge_s^0	V^+	(Ge-V) ⁺	7.5
As_s^0	V^-	(As-V) ⁻	10.4	As_s^+	V^0	(As-V) ⁺	4.6
Se_s^0	V^-	(Se-V) ⁻	11.8	Se_s^+	V^0	(Se-V) ⁺	8.6
Br_s^0	V^-	(Br-V) ⁻	12.8	Br_s^+	V^0	(Br-V) ⁺	10.1
In_s^-	V^0	(In-V) ⁻	8.7	In_s^0	V^+	(In-V) ⁺	9.7
Sn_s^0	V^-	(Sn-V) ⁻	9.1	Sn_s^0	V^+	(Sn-V) ⁺	8.9
Sb_s^0	V^-	(Sb-V) ⁻	13.6	Sb_s^+	V^0	(Sb-V) ⁺	8.2
Te_s^0	V^-	(Te-V) ⁻	14.0	Te_s^+	V^0	(Te-V) ⁺	12.4
I_s^0	V^-	(I-V) ⁻	14.8	I_s^+	V^0	(O-V) ⁺	14.4

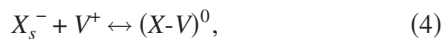


However, V has an $(-/0)$ level at $E_c - 2.65$ eV,⁵⁷ and there is evidence for a positively charged vacancy in irradiated B-doped material.^{30,58} The precise location of the $(0/+)$ is not established, but previous computational studies predicted the $(0/+)$ level to be 1.7–1.9 eV above the valence-band top,^{23,59} with a second $(0/+)$ level lying a few tenths of an eV below the first. However, these values are derived using a charge-state-dependent formation energy without correcting for the complex multiplet character of the vacancy^{53,55} or for the effects of having a periodic boundary condition.⁶⁰ Both corrections would tend to lower the $(0/+)$ level. We have recently performed calculations where we compare the ionization energies of different systems to estimate the $(0/+)$ levels, and we found that the $(0/+)$ level of V is likely to be close to the valence-band top.¹⁶

The three likely charge states of V permit the reaction



such as would be expected for $X=P$, and



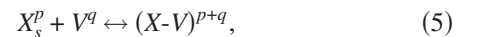
such as for $X=B$.

The binding energies for these reactions differ from in Table III by the difference in the appropriate $(0/+)$ and $(-/0)$ levels. E^b allowing for dissociation of $(X-V)^0$ into charged species is included in Fig. 7. E^b for charged systems depends on the accuracy of the electrical levels of $X-V$, X_s , and V , which constitutes a considerable difficulty since the $(0/+)$ level of V has a theoretical range of $E_v + 0.3 - 1.9$ eV.

The data in Fig. 7 use the highest value, $E_v + 1.9$ eV,²³ and where available, we have used experimental electrical levels for other systems.

In the likely event that V has a $(0/+)$ level lower in the gap than predicted by Baskin *et al.*,²³ $X-V$ dissociation will not involve V^+ (e.g., Al- V dissociates into V^0 and Al_s^0 rather than V^+ and Al_s^-), with the possible exception of B- V . Dissociation into charged defects does not greatly affect the chemical trends.

In addition to reactions involving $(X-V)^0$ complexes, it remains to examine reactions of the type



where $p+q \neq 0$. As with the reactions in Eqs. (3) and (4), the binding energy associated with Eq. (5) can also be estimated by combining the electrical levels with the binding energy for reaction in Eq. (2). Table IV lists the calculated binding energies for various reactions described by Eq. (5), which are also plotted in Fig. 7. These data show the same trends as for the neutral species, further suggesting that impurity size is the most important consideration.

6. Correlation of $(X-V)$ complexes with experiment

In some cases there is experimental evidence for the existence of $X-V$ complexes. The N- V and Si- V complexes are well established and not discussed here.

a. B- V . An EPR center with $S=1$ has been correlated with boron: W36 is seen in natural semiconducting material and has trigonal symmetry and a zero-field-splitting parameters of 103.4 MHz along the C_3 axis.^{61,62}

The calculated spin-spin zero-field-splitting parameters for $(B-V)^-$ are $D_{\parallel}=1255$ MHz and $D_{\perp}=-628$ MHz. Although this calculation in itself cannot rule out a correlation between W36 and $(B-V)^-$, we note that for self-interstitial defects in diamond as well as vacancy-related defects in silicon the agreement between the calculated and experimental D -tensor magnitudes is much better than this.^{43,63} Furthermore, $(N-V)^-$, which electronically resembles $(B-V)^-$ in terms of the spin density, is the W15 EPR center which has measured zero-field-splitting components of $D_{\parallel}=1920$ MHz and $D_{\perp}=-960$ MHz,⁶⁴ and our calculations yield $D_{\parallel}=2145$ MHz and $D_{\perp}=-1073$ MHz. This tends to rule out $(B-V)^-$ as a model for W36.

The small values of the D -tensor components may indicate that the defect responsible consists of two spins that are more spatially separated than in the dangling bonds of the vacancy.

There have also been electrical levels detected in B-containing material.^{65,66} They lie at 1.30 ± 0.10 eV, 1.14 ± 0.05 eV (Ref. 66) and $E_v+1.25$ eV (Ref. 65). We previously suggested that these may be related to boron pairs,⁴⁵ but these levels are also consistent with B-V complexes (Table III). Additional experimental data, such as available from EPR, would be required to distinguish which, if either, of these models is correct.

b. O-V. Oxygen has also been (tentatively) assigned to orthorhombic-I EPR centers ($R5-R11$),⁶⁴ many models being oxygen-vacancy aggregates. Although it appears there is no direct evidence of oxygen in any of these centers, we note that $R9$ has been assigned to $(O-V)$.⁶⁴ $R9$ has either $S=1$ or $S=3/2$. As indicated in Table III, we find that $(O-V)^0$ has $S=1$ in the ground state, but the symmetry is inconsistent with $R9$ and, indeed, with $R5-R11$. In order to obtain the correct symmetry for $(O-V)$, the O atom would have to be a more distant neighbor to the vacancy, which we find to be energetically unfavorable.

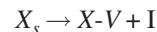
c. In-V. Channeling studies of indium-implanted material suggest the presence of In-V complexes. The dominant non-substitutional defect is interpreted in terms of a displaced In atom around 0.45 Å from a substitutional site along $\langle 111 \rangle$ towards a bond-centered site.⁶⁷ We calculate that, even when complexed with a lattice vacancy, there is a considerable volume displaced, indicating that multivacancy complexes would be required to completely accommodate the size of the In ion, consistent with the conclusions of Ref. 67.

IV. CONCLUSIONS

We have examined the electronic structure and electrical properties of a wide range of substitutional impurities and their complexes with lattice vacancies in diamond. In most cases the electronic structure of the substitutional impurities can be understood from the vacancy model⁶⁸ and also for the $X-V$ centers. Although all defects have deep levels in the band gap, surprisingly there are a number of cases, such as

$S-V$, which are likely to be optically and magnetically inactive, rendering them hard to identify.

The energetics of the complex formation have important implications for doping. For very large impurities (such as the fourth-row elements) the binding energy of the vacancy to the impurity is extremely large, with the maximal value being around 15 eV for Te-V and I-V. Once formed, the barrier to dissociation can be approximated by the sum of the binding energy and migration barrier for the lattice vacancy—i.e., above 17 eV. However, even for these extreme cases, the binding energy is insufficient to render the reaction



exothermic, since this would require $\Delta E^f > E^f I$: our calculated values of $\Delta E^f \leq 10$ eV, whereas the formation energy of the self-interstitial is theoretically around 12–13 eV.^{43,69}

Nevertheless, thermodynamically there is a large driving force to produce $X-V$ complexes for “large” impurities such as As and Sb. Whether this is true during growth is not clear, and it is possible that nonequilibrium concentrations of these substitutional impurities may be incorporated, as appears to be the case for P_s . In contrast with P, As and Sb are much more stable when complexed with vacancies, suggesting that the nonequilibrium incorporation of these potentially shallower donors is less likely.

The alternative, intrinsically nonequilibrium doping method of ion implantation remains a possibility. A typical scheme involves the introduction of the dopant species followed by a thermal anneal to remove unwanted lattice disorder. This process might be expected to work for boron-implanted material due to the relatively weakly bound $B-V$. In contrast for the larger donor species, even if a large fraction of impurities are initially at substitutional sites, it seems likely that the considerable binding energies of V to (for instance) As and Sb will drive the reaction in Eq. (3) to the right. Once formed, they will be very difficult to anneal out, if they can be removed at all: for As-V the dissociation barrier is estimated from above to be >11 eV. Since the $X-V$ complexes are compensating defects, even at 50% on-site donors, the presence of unannealed damage is likely to lead to very low carrier concentrations. In addition, ionized defects will reduce carrier mobility. Both low donor concentration and mobility are consistent with typical observations following implantation doping.

In summary, the large binding energy and electrical activity of $X-V$ complexes are important limiting factors in the formation of n -type material, especially via ion implantation. However, the presence of such systems should be able to be determined experimentally via EPR and optical experiments in many cases.

ACKNOWLEDGMENT

The authors acknowledge the EPSRC for financial support.

- ¹P. A. Crowther, P. J. Dean, and W. F. Sherman, *Phys. Rev.* **154**, 772 (1967).
- ²E. Bustarret, E. Gheeraert, and K. Watanabe, *Phys. Status Solidi A* **199**, 9 (2003).
- ³E. Gheeraert, S. Koizumi, T. Teraji, and H. Kanda, *Solid State Commun.* **113**, 577 (2000).
- ⁴I. Sakaguchi, M. N. Gamo, Y. Kikuchi, E. Yasu, H. Haneda, T. Suzuki, and T. Ando, *Phys. Rev. B* **60**, R2139 (1999).
- ⁵S. Gupta, B. R. Weiner, and G. Morell, *Appl. Phys. Lett.* **83**, 491 (2003).
- ⁶K. Nakazawa, M. Tachiki, H. Kawarada, A. Kawamura, K. Horiuchi, and T. Ishikura, *Appl. Phys. Lett.* **82**, 2074 (2003).
- ⁷Z. Teukam, J. Chevallier, C. Saguy, R. Kalish, D. Ballutaud, M. Barbé, F. Jomard, A. Tromson-Carli, C. Cytermann, J. E. Butler, M. Bernard, C. Baron, and A. Deneuveille, *Nat. Mater.* **2**, 482 (2003).
- ⁸A. B. Anderson, E. J. Grantscharova, and J. C. Angus, *Phys. Rev. B* **54**, 14341 (1996).
- ⁹T. Miyazaki, H. Okushi, and T. Uda, *Phys. Rev. Lett.* **88**, 066402 (2002).
- ¹⁰T. Miyazaki, H. Okushi, and T. Uda, *Appl. Phys. Lett.* **78**, 3977 (2001).
- ¹¹T. Miyazaki and H. Okushi, *Diamond Relat. Mater.* **11**, 323 (2002).
- ¹²T. V. Albu, A. B. Anderson, and J. C. Angus, *J. Electrochem. Soc.* **149**, E143 (2002).
- ¹³T. Nishimatsu, H. Katayama-Yoshida, and N. Orita, *Physica B* **302–303**, 149 (2001).
- ¹⁴D. Segev and S.-H. Wei, *Phys. Rev. Lett.* **91**, 126406 (2003).
- ¹⁵S. J. Sque, R. Jones, J. P. Goss, and P. R. Briddon, *Phys. Rev. Lett.* **92**, 017402 (2004).
- ¹⁶J. P. Goss, P. R. Briddon, S. J. Sque, and R. Jones, *Diamond Relat. Mater.* **13**, 684 (2004).
- ¹⁷T. Miyazaki and H. Okushi, *Diamond Relat. Mater.* **10**, 449 (2001).
- ¹⁸R. Kalish and C. Uzan-Saguy, in *Properties, Growth and Applications of Diamond*, No. 26 in *EMIS Datareviews Series*, edited by M. H. Nazaré and A. J. Neves (INSPEC, Institute of Electrical Engineers, London, 2001), Chap. B3.1, pp. 321–330.
- ¹⁹J. D. Hunn, N. R. Parikh, M. L. Swanson, and R. A. Zuhr, *Diamond Relat. Mater.* **2**, 847 (1993).
- ²⁰J. F. Prins, *Diamond Relat. Mater.* **4**, 580 (1995).
- ²¹R. Kalish, C. Uzan-Saguy, R. Walker, and S. Prawer, *J. Appl. Phys.* **94**, 3923 (2003).
- ²²J. F. Prins, *Diamond Relat. Mater.* **11**, 612 (2002).
- ²³E. Baskin, A. Reznik, D. Saada, J. Adler, and R. Kalish, *Phys. Rev. B* **64**, 224110 (2001).
- ²⁴H. Quintel, K. Bharuth-Ram, H. Hofsäss, M. Restel, and C. Ronning, *Nucl. Instrum. Methods Phys. Res. B* **118**, 72 (1996).
- ²⁵J. G. Correia, J. G. Marques, E. Alves, D. Forkel-Wirth, S. G. Jahn, M. Restle, M. Dalmer, H. Hofsäss, K. Bharuth-Ram, and ISOLDE Collaboration, *Nucl. Instrum. Methods Phys. Res. B* **127–128**, 723 (1997).
- ²⁶J. P. Goss, R. Jones, S. J. Breuer, P. R. Briddon, and S. Öberg, *Phys. Rev. Lett.* **77**, 3041 (1996).
- ²⁷G. Davies and M. F. Hamer, *Proc. R. Soc. London, Ser. A* **348**, 285 (1976).
- ²⁸G. Davies, *J. Phys. C* **12**, 2551 (1979).
- ²⁹Y. Mita, *Phys. Rev. B* **53**, 11360 (1996).
- ³⁰J. W. Steeds, S. J. Charles, J. Davies, and I. Griffin, *Diamond Relat. Mater.* **9**, 397 (2000).
- ³¹J. H. N. Loubser and J. A. van Wyk, *Rep. Prog. Phys.* **41**, 1201 (1978).
- ³²C. D. Clark, H. Kanda, I. Kiflawi, and G. Sittas, *Phys. Rev. B* **51**, 16681 (1995).
- ³³K. Iakoubovskii, G. J. Adriaenssens, and M. Nesladek, *J. Phys.: Condens. Matter* **12**, 189 (2000).
- ³⁴D. J. Twitchen, M. E. Newton, J. M. Baker, T. R. Anthony, and W. F. Banholzer, *Phys. Rev. B* **59**, 12900 (1999).
- ³⁵B. J. Coomer, A. Resende, J. P. Goss, R. Jones, S. Öberg, and P. R. Briddon, *Physica B* **273–274**, 520 (1999).
- ³⁶R. Jones, J. E. Lowther, and J. Goss, *Appl. Phys. Lett.* **69**, 2489 (1996).
- ³⁷B. P. Doyle, J. K. Dewhurst, J. E. Lowther, and K. Bharuth-Ram, *Phys. Rev. B* **57**, 4965 (1998).
- ³⁸R. Jones and P. R. Briddon, in *Identification of Defects in Semiconductors*, Vol. 51A of *Semiconductors and Semimetals*, edited by M. Stavola (Academic Press, Boston, 1998), Chap. 6.
- ³⁹H. J. Monkhorst and J. D. Pack, *Phys. Rev. B* **13**, 5188 (1976).
- ⁴⁰C. Hartwigsen, S. Goedecker, and J. Hutter, *Phys. Rev. B* **58**, 3641 (1998).
- ⁴¹D. A. Liberman, *Phys. Rev. B* **62**, 6851 (2000).
- ⁴²A. Resende, R. Jones, S. Öberg, and P. R. Briddon, *Phys. Rev. Lett.* **82**, 2111 (1999).
- ⁴³J. P. Goss, B. J. Coomer, R. Jones, T. D. Shaw, P. R. Briddon, M. Rayson, and S. Öberg, *Phys. Rev. B* **63**, 195208 (2001).
- ⁴⁴M. J. Rayson, Ph.D. thesis, School of Physical Sciences, University of Newcastle upon Tyne, 2005.
- ⁴⁵J. P. Goss, P. R. Briddon, R. Jones, Z. Teukam, D. Ballutaud, F. Jomard, J. Chevallier, M. Bernard, and A. Deneuveille, *Phys. Rev. B* **68**, 235209 (2003).
- ⁴⁶H. Kim, A. K. Ramdas, S. Rodriguez, M. Grimsditch, and T. R. Anthony, *Phys. Rev. Lett.* **83**, 4140 (1999).
- ⁴⁷Pan Bacai and X. Shangda, *Phys. Rev. B* **49**, 11444 (1994).
- ⁴⁸E. B. Lombardi, A. Mainwood, K. Osuch, and E. C. Reynhardt, *J. Phys.: Condens. Matter* **15**, 3135 (2003).
- ⁴⁹A. Gali, J. E. Lowther, and P. Deák, *J. Phys.: Condens. Matter* **13**, 11607 (2001).
- ⁵⁰K. L. Brower, *Phys. Rev. B* **4**, 1968 (1971).
- ⁵¹C. Kittel, *Introduction to Solid State Physics*, 8th ed. (Wiley, Chichester, 2005).
- ⁵²R. Farrer, *Solid State Commun.* **7**, 685 (1969).
- ⁵³C. A. Coulson and M. J. Kearsley, *Proc. R. Soc. London, Ser. A* **241**, 433 (1957).
- ⁵⁴C. A. Coulson and F. P. Larkins, *J. Phys. Chem. Solids* **30**, 1963 (1969).
- ⁵⁵R. Q. Hood, P. R. C. Kent, R. J. Needs, and P. R. Briddon, *Phys. Rev. Lett.* **91**, 076403 (2003).
- ⁵⁶Y. Yan, S. B. Zhang, and M. M. Al-Jassim, *Phys. Rev. B* **66**, 201401(R) (2002).
- ⁵⁷S. Dannefaer, A. Pu, and D. Kerr, *Diamond Relat. Mater.* **10**, 2113 (2001).
- ⁵⁸S. J. Charles, J. W. Steeds, J. E. Butler, and D. J. F. Evans, *J. Appl. Phys.* **94**, 3091 (2003).
- ⁵⁹J. Bernholc, A. Antonelli, T. M. Del Sole, Y. Bar-Yam, and S. T. Pantelides, *Phys. Rev. Lett.* **61**, 2689 (1988).
- ⁶⁰G. Makov and M. C. Payne, *Phys. Rev. B* **51**, 4014 (1995).
- ⁶¹J. H. N. Loubser and J. A. van Wyk (unpublished).
- ⁶²J. M. Baker and M. E. Newton, *Appl. Magn. Reson.* **7**, 209 (1994).

- ⁶³M. J. Rayson, J. P. Goss, and P. R. Briddon, *Physica B* **340–342**, 673 (2003).
- ⁶⁴C. A. J. Ammerlaan, in *Semiconductors*, edited by O. Madelung, Landolt-Börnstein, New Series, Group III, Vol. 22, Pt. b (Springer, Berlin, 1998).
- ⁶⁵C. E. Nebel, R. Zeisel, and M. Stutzmann, *Phys. Status Solidi A* **174**, 117 (1999).
- ⁶⁶P. Muret, E. Gheeraert, and A. Deneuveville, *Phys. Status Solidi A* **174**, 129 (1999).
- ⁶⁷B. P. Doyle, E. J. Storbeck, U. Wahl, S. H. Connell, J. P. F. Sellschopp, and the ISOLDE Collaboration, *J. Phys.: Condens. Matter* **12**, 67 (2000).
- ⁶⁸G. D. Watkins, *Physica B & C* **117–118**, 9 (1983).
- ⁶⁹J. P. Goss, R. Jones, and P. R. Briddon, *Phys. Rev. B* **65**, 035203 (2002).